Eur. Phys. J. C 26, 357–370 (2003)
Digital Object Identifier (DOI) 10.1140/epjc/s2002-01073-6

THE EUROPEAN PHYSICAL JOURNAL C

V^0, $\overline{\Xi}^+$ and Ω^- inclusive production cross sections measured in hyperon experiment WA89 at CERN

The WA89 Collaboration

M.I. Adamovich[8], Yu.A. Alexandrov[8,a], S.P. Baranov[8,a], D. Barberis[3], M. Beck[5], C. Bérat[4], W. Beusch[2], M. Boss[6], S. Brons[5,b], W. Brückner[5], M. Buénerd[4], Ch. Busch[6], Ch. Büscher[5], F. Charignon[4], J. Chauvin[4], E.A. Chudakov[6,c], U. Dersch[5], F. Dropmann[5], J. Engelfried[6,d], F. Faller[6,e], A. Fournier[4], S.G. Gerassimov[8,f], M. Godbersen[5], P. Grafström[2], Th. Haller[5], M. Heidrich[5], E. Hubbard[5], R.B. Hurst[3], K. Königsmann[5,g], I. Konorov[5,8,f], N. Keller[6], K. Martens[6,h], Ph. Martin[4], S. Masciocchi[5,i], R. Michaels[5,c], U. Müller[7], H. Neeb[5], D. Newbold[1], C. Newsom[j], S. Paul[5,f], J. Pochodzalla[5,k] I. Potashnikova[5], B. Povh[5], R, Ransome[l], Z. Ren[5], M. Rey-Campagnolle[4,m], G. Rosner[7], L. Rossi[3], H. Rudolph[7], C. Scheel[n], L. Schmitt[7,f], H.-W. Siebert[6], A. Simon[6,g], V. Smith[1,o], O. Thilmann[6], A. Trombini[5], E. Vesin[4], B. Volkemer[7], K. Vorwalter[5], Th. Walcher[7], G. Wälder[6], R. Werding[5], E. Wittmann[5], M.V. Zavertyaev[8,a]

[1] University of Bristol, Bristol, UK
[2] CERN, 1211 Genève 23, Switzerland
[3] Genoa Univ./INFN, Dipt. di Fisica, 16146 Genova, Italy
[4] Grenoble ISN, 38026 Grenoble, France
[5] Heidelberg Max-Planck-Institut für Kernphysik, Postfach 103980, 69029 Heidelberg, Germany
[6] Universität Heidelberg, Physikalisches Institut, 69120 Heidelberg, Germany[p]
[7] Universität Mainz, Inst. für Kernphysik, 55099 Mainz, Germany
[8] Moscow Lebedev Physics Inst., 117924, Moscow, Russia

Received: 14 February 2002 / Revised version: 9 October 2002 /
Published online: 9 December 2002 –

Abstract. We report on a measurement of the inclusive cross sections of Λ, $\overline{\Lambda}$, K^0_S, $\overline{\Xi}^+$ and Ω^- production by $\Sigma^-$and $\pi^-$of 345 GeV/c momentum and by neutrons of 260 GeV/c mean momentum in copper and carbon. The differential cross sections as function of p_t^2 show a distinct non-gaussian behavior above 1.2 $(\mathrm{GeV}/c)^2$. A comparison of the x_F-dependence of Λ, $\overline{\Lambda}$ and K^0 production with calculations using PYTHIA and the QGSM model is discussed.

1 Introduction

Hadron production in hadron beams has already been studied in a variety of beams for a wide range of produced hadrons. However, data on the production of the hyperons discussed in this article (Λ, $\overline{\Lambda}$, K^0_S, $\overline{\Xi}^+$ and Ω^-) are still rather limited.

The production of V^0 (Λ, $\overline{\Lambda}$ and K^0_S) have been studied by some experiments with a proton beam [1]–[13]) over a wide momentum range 6–800 GeV/c. A few experiments

[a] Supported by Deutsche Forschungsgemeinschaft, contract number DFG 436 RUS 113/465/0-2(R), and Russian Foundation for Basic Research under contract number RFFI 00-02-04018

[b] Now at TRIUMF, Vancouver, B.C., Canada V6T 2A3

[c] Now at Thomas Jefferson Lab, Newport News, VA 23606, USA

[d] Now at Instituto de Fisica, Universidad Autonoma de San Luis Potosi, S.L.P. 78240 Mexico

[e] Now at Fraunhofer Inst. für Solar Energiesysteme, 79100 Freiburg, Germany

[f] Now at Technische Universität München, Garching, Germany

[g] Now at Fakultät für Physik, Universität Freiburg, Germany

[h] Now at Departament of Physics and Astronomy, SUNY at Stony Brook, NY 11794-3800, USA

[i] Now at Max-Planck-Institut für Physik, München, Germany

[j] University of Iowa, Iowa City, IA 52242, USA

[k] Universitaät Mainz, Institut für Kernphysik, Germany

[l] Rutgers University, Piscataway, NJ 08854, USA

[m] *Permanent address:* CERN, 1211 Genève 23, Switzerland

[n] NIKEF, 1009 DB Amsterdam, The Netherlands

[o] Supported by the UK PPARC

[p] Supported by the Bundesministerium für Bildung, Wissenschaft, Forschung und Technologie, Germany, under contract numbers 05 5HD15I, 06 HD524I and 06 MZ5265

were performed with a pion beam [14]–[17] in the narrow momentum range of 100–360 GeV/c. One experiment was done with kaon beam [18] at 200 GeV/c and neutrons [19] at average momentum of 45 GeV/c. Most of these experiments were done with bubble chambers and consequently have a low statistics. No data on V^0 production in hyperon beams exist.

Ω^- production was studied in K^--beams [20]–[23] at very low momentum 4.5–14 GeV/c and in a Ξ^- beam [25] at 116 GeV/c. In the pion beam the combined production of ($\Xi^- + \overline{\Xi}^+$) was studied at 200 GeV/c [14]. $\overline{\Xi}^+$ and Ω^- production cross section were also measured in proton beams of 400 GeV/c [26].

Progress in heavy ion physics has renewed interest in studies of strange-particle production. The new generation of heavy ion colliders target the observation of quark-gluon plasma (QGP) in experiments such as PHENIX [27] and STAR [28] at RHIC. One of the most promising signatures of QGP formation should be an enhanced production of strange particles [29]. These expectations lend importance to a comprehensive measurement of strange particle production properties in "ordinary" pN collisions.

The x_F[1] and p_t^2 spectra contain important information on the production mechanisms. The x_F spectra provide information about the underlying hadron interaction dynamics, for instance the "leading" particle effect, while the p_t^2 spectra contain information about the thermal equilibrium if it has been reached.

In this paper we present the results of the inclusive cross sections studies of Λ, $\overline{\Lambda}$, K^0_S, $\overline{\Xi}^+$ and Ω^- produced by $\Sigma^-$and $\pi^-$of 345 GeV/c momentum and by neutrons of 260 GeV/c mean momentum in copper and carbon.

2 Hyperon beam and experimental apparatus

The hyperon beam was derived from an external proton beam of the CERN-SPS, hitting a hyperon production target placed 16 m upstream of the experimental target. Negative secondaries with a mean momentum of 345 GeV/c and a momentum spread $\sigma(p)/p \approx 9\%$ were selected in a magnetic channel. The production angles relative to the proton beam were smaller than 0.5 mrad. At the experimental target, the beam consisted of π^-, K^-, Σ^- and Ξ^- in the ratio 2.3: 0.025: 1: 0.008. A transition radiation detector (TRD) made of 10 MWPCs interleaved with foam radiators allows π^- to be suppressed at the trigger level with the efficiency of (95 ± 2) while keeping (82 ± 1) of the Σ^-'s [30]. Typically, about $1.8 \cdot 10^5$ Σ^- and $4.5 \cdot 10^5$ π^- were delivered to the target during one SPS-spill, which had an effective length of about 1.5 s.

Σ^- decays upstream of the target are a source of neutrons which were used in our measurement as a neutron beam. The momenta of these neutrons were defined as the difference between the average Σ^- momentum and the momentum of the associated π^- measured in the spectrometer. The neutron spectrum has an average momentum of 260 GeV/c and a width of $\sigma(p)/p = 15\%$. More details can be found in [31].

The experimental target consisted of one copper and three carbon (poly-cristaline diamond) blocks arranged in a row along the beam. Each copper and carbon block had a thickness corresponding to an interaction length of 2.6% and 0.83%, respectively. At the target, the beam had a width of 3 cm and a height of 1.7 cm. Microstrip detectors upstream and downstream of the target allowed the tracks of the incoming beam particle and of the charged particles produced in the target blocks to be measured. The target was positioned 14 m upstream of the center of the Omega spectrometer magnet [32] so that a field-free decay region of 10 m length was provided for hyperon and K^0_S decays. Tracks of charged particles were measured inside the magnet and in the field-free regions upstream and downstream by MWPCs and drift-chambers, with a total of 130 planes. The Omega magnet provided a field integral of 7.5 Tm, and the momentum resolution achieved was $\sigma(p)/p^2 \approx 10^{-4}$ (GeV/c)$^{-1}$.

A ring-imaging Cherenkov detector, an electromagnetic calorimeter and a hadron calorimeter were placed downstream of the spectrometer. They were not used in the analysis presented here.

The main trigger selected about 25% of all interactions, using multiplicities measured in microstrip counters upstream and downstream of the target, and in scintillator hodoscopes and MWPCs behind the Omega magnet. Correlations between hits in different detectors were used in the trigger to increase the fraction of events with high-momentum particles, thus reducing background from low-momentum pions in the beam. In addition, a reduced sample of beam triggers was recorded for trigger calibration purposes. The results presented in this article are based on 100 million events recorded in 1993.

3 Event selection

In the following, we describe the reconstruction of the beam-target interaction vertex, the search for V^0 candidates and finally the search for $\overline{\Xi}^+$ and Ω^- candidates.

The interaction vertex had to contain at least two outgoing charged tracks reconstructed in the microstrip counters downstream of the target. The reconstructed vertex position had to be within a target block where in each coordinate an additional margin of 3σ was allowed, i.e 1.6 mm in the beam direction and 75 μm in the transverse direction.

For Σ^- and π^- interactions, the beam track reconstructed in the microstrip counters upstream of the target had to have a transverse distance to the reconstructed interaction vertex of less than 6σ ($\sigma \approx 25\,\mu$m).

For neutron interactions the beam track interpreted as the π^- track from a Σ^- decay had to have a transverse distance to the interaction vertex of more than 6σ. In addition, this assumed π^- track had to be connected

[1] The Feynman variable defines as: $x_F = 2p^*_{\parallel}/\sqrt{s}$. Here the $p_{\parallel}$ is the longitudinal momentum of the particle in the CMS and s is the center of mass energy

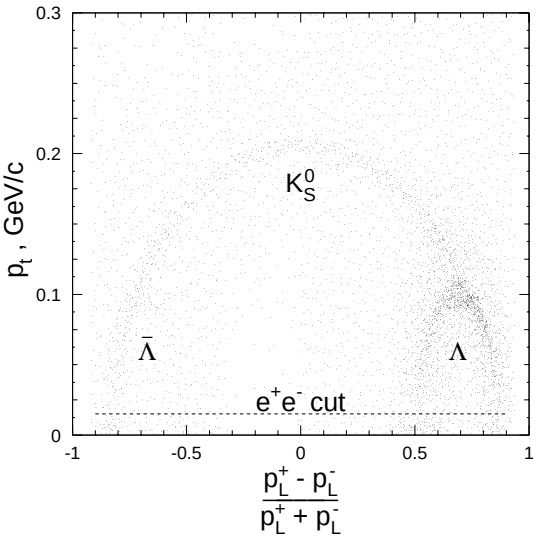

Fig. 1. Armenteros-Podolanski plot of the V^0. e^+e^- pairs were cut at $p_t = 0.015$ GeV/c. $p_L^{\pm}$ and p_t are the laboratory longitudinal and transverse momenta of the decay tracks with the respect to the V^0 direction

to a track in the spectrometer corresponding to a negative particle with a momentum smaller than 140 GeV/c corresponding to the $\Sigma^- \rightarrow n\pi^-$ decay kinematics at $< p > \approx$ 345 GeV/c. These cuts were optimized to separate $\Sigma^-$and π^-interactions from neutron interactions.

V^0 candidates then were selected from all pairs of positive and negative tracks which formed a vertex in the decay zone (-1332 ÷ -332 cm) between the microstrip detectors (50 cm downstream of the target) and the Omega magnet (decay length of 10 m). The distance between the two tracks at the decay point had to be smaller than 3 mm. The V^0 trajectory reconstructed from the decay particles had to have a transverse distance to the interaction vertex of less than 12 mm. The reconstructed V^0 mass had to be within $5\sigma_m$ and 15 MeV/c^2 of the world mass average of the corresponding V^0, the mass error σ_m being typically 2 MeV/c^2 for Λ and $\overline{\Lambda}$ and 4 MeV/c^2 for K^0_S. The V^0 momentum had to be below 260 GeV/c.

The background from $\gamma \rightarrow e^+e^-$conversion was suppressed on the basis of the Armenteros plot (Fig. 1) by requiring that the transverse momenta of the decay tracks with the respect to the V^0 direction be greater than 15 MeV/c.

For the selection of $\overline{\Xi}^+$ and Ω^- candidates, $\overline{\Lambda}$ and Λ candidates with a reconstructed mass within $3\sigma_m$ of the $\overline{\Lambda}$ or Λ mass were combined with positive or negative tracks respectively. These tracks had to form a $\Omega^-/\overline{\Xi}^+$ decay vertex within the same decay zone as V^0, with the V^0 decay vertex downstream at a distance of at least 3σ (typically 14 cm). For $\Omega^- \rightarrow \Lambda K^-$ decay candidates the reconstructed $\Lambda\pi^-$ effective mass had to be larger than 1340 MeV/c^2 to suppress the background from $\Xi^- \rightarrow \Lambda\pi^-$ decays.

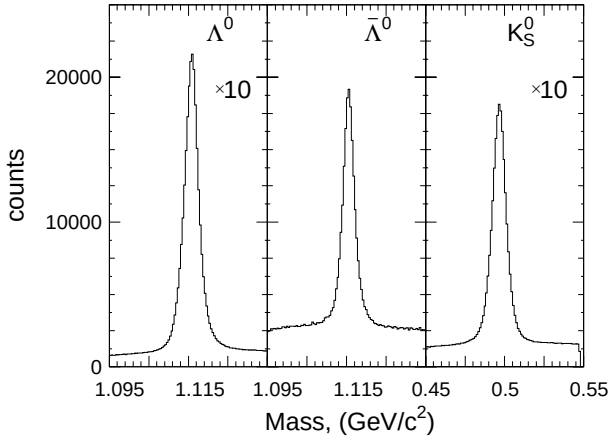

Fig. 2. The effective mass distribution of V^0 produced in Σ^- beam

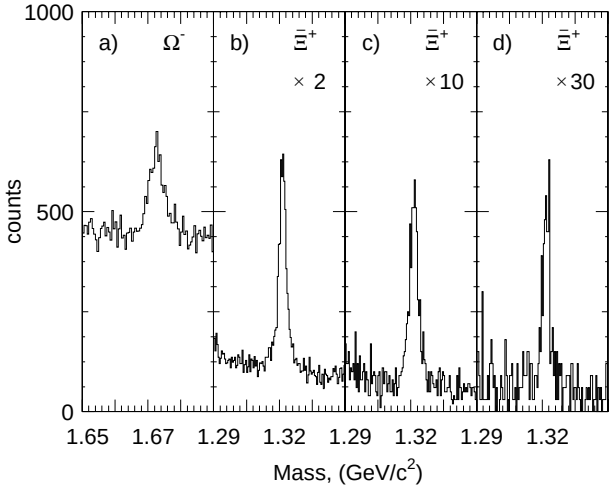

Fig. 3a–d. Effective mass distribution of $\overline{\Lambda}\pi^+$and ΛK^- combinations

4 Observed signals

Figure 2 shows the mass distributions for all V^0 candidates with $x_F > 0$ produced in Σ^- interactions. Clear signals of V^0 decays are visible above low backgrounds. Figure 3a shows the effective mass distribution of the Ω^- candidates produced by Σ^- and Figs. 3b–d show the effective mass distributions of $\overline{\Xi}^+$ candidates produced by Σ^- , neutrons and π^-correspondingly. The signal sample sizes were estimated by fitting combinations of a Gaussian with a Legendre polynomial up to 3rd order to the effective mass distributions, with the resulting numbers given in Table 1.

5 Production cross section

The differential production cross section as a function of the Feynman variable, x_F, and the squared transverse momentum, p_t^2, was calculated using the following formula:

$$\sigma(x_F, p_t^2) = \frac{1}{BR_{Hyp}} \cdot \frac{N_{Hyp}}{\varepsilon(x_F, p_t^2)\ N_b\ \rho\ l\ N_A/M}. \quad (1)$$

Table 1. The number of reconstructed events and total inclusive hyperon production cross sections per nucleus and nucleon. The α is the exponent in the cross section parametrization vs. atomic number of the form A^α

particle	target	statistic	σ_{nucl} [mb]	σ_0 [mb]	α
			Σ^- beam		
Λ	Cu	1162398 ± 1157	$110. \pm 4.$		
	C	1132019 ± 1140	$41. \pm 2.$		
	nucleon			9.5 ± 0.5	0.59 ± 0.03
$\overline{\Lambda}$	Cu	79779 ± 339	7.0 ± 0.5		
	C	70913 ± 324	2.2 ± 0.2		
	nucleon			0.39 ± 0.03	0.69 ± 0.05
K^0	Cu	938450 ± 1085	$67. \pm 4.$		
	C	870884 ± 1047	$22. \pm 1.$		
	nucleon			4.3 ± 0.2	0.66 ± 0.03
$\overline{\Xi}^+$	Cu	1245 ± 43	0.64 ± 0.02		
	C	1109 ± 42	0.18 ± 0.01		
	nucleon			0.023 ± 0.002	0.77 ± 0.04
Ω^-	Cu	1630 ± 99	0.63 ± 0.04		
	C	1239 ± 84	0.17 ± 0.01		
	nucleon			0.024 ± 0.003	0.78 ± 0.06
			π^- beam		
Λ	Cu	31369 ± 211	$25. \pm 1.$		
	C	27367 ± 197	7.9 ± 0.4		
	nucleon			1.5 ± 0.1	0.68 ± 0.03
$\overline{\Lambda}$	Cu	12501 ± 135	11.9 ± 0.7		
	C	10424 ± 125	3.6 ± 0.2		
	nucleon			0.59 ± 0.04	0.72 ± 0.05
K^0	Cu	77274 ± 309	$53. \pm 3.$		
	C	68589 ± 292	$17. \pm 1.$		
	nucleon			3.2 ± 0.2	0.68 ± 0.05
$\overline{\Xi}^+$	Cu	272 ± 19	1.3 ± 0.1		
	C	241 ± 17	0.45 ± 0.03		
	nucleon			0.07 ± 0.1	0.61 ± 0.07
			neutron beam		
Λ	Cu	34997 ± 199	$56. \pm 3.$		
	C	30585 ± 186	$18. \pm 1.$		
	nucleon			3.4 ± 0.2	0.68 ± 0.04
$\overline{\Lambda}$	Cu	4285 ± 76	7.7 ± 0.6		
	C	3741 ± 71	2.4 ± 0.2		
	nucleon			0.42 ± 0.03	0.69 ± 0.05
K^0	Cu	34456 ± 205	$52. \pm 3.$		
	C	30609 ± 193	$17. \pm 1.$		
	nucleon			2.9 ± 0.2	0.69 ± 0.04
$\overline{\Xi}^+$	Cu	59 ± 9	1.4 ± 0.3		
	C	51 ± 9	0.31 ± 0.05		
	nucleon			0.012 ± 0.002	0.8 ± 0.2

Here N_{Hyp} is the number of observed hyperons in the particular region of the corresponding kinematic variables and ε denotes the overall acceptance including reconstruction and trigger efficiencies. N_b is the number of incoming beam particles tagged as Σ^-, π^- or neutron, corrected for corresponding beam contaminations (see below) and for losses due to the dead time of the trigger and the data acquisition system. M, ρ and l are the atomic mass, the density and the length of the target, N_A is the Avogadro number. The branching ratio of hyperon into the measured decay channel was taken from [33].

From our previous studies [31] we know that our Σ^-, π^- and neutron interaction samples have several contaminations which have to be taken into account. The correction for the Σ^- contamination in the π^- interaction sample and vice versa was done iteratively. The total remaining contamination of the Σ^- in the π^- beam was determined as $(1.5 \pm 1)\%$ and $(12.3 \pm 0.5)\%$ of the π^- contamination in the Σ^- beam [24]. Since the contamination level in π^- beam is quite low we used the uncorrected production cross sections measured in π^- beam as a first level correction to the production cross section measured in the Σ^- beam. Then the corrected production cross section in the Σ^- beam was used for the corrections for π^- beam. The procedure converges after two iterations. The Ξ^- and K^- contaminations in the Σ^- interaction sample have to be considered individually.

The Ξ^- contamination in the Σ^- interaction samples was measured to be $(1.3 \pm 0.3)\%$. For the correction we used the cross section of Ω^- production by Ξ^- of 130 GeV/c momentum measured in the previous hyperon beam experiment [25]. The cross sections for V^0 or $\overline{\Xi}^+$ production in Ξ^- induced interactions have never been measured. Instead we used our measured production cross sections in the Σ^- interaction. We suppose that the following approximate relations between the cross sections can be used:

a) $\sigma(\Xi \to \Lambda) = 2\sigma(\Sigma \to \Lambda)$ and $\sigma(\Xi \to K^0_s) = 2\sigma(\Sigma \to K^0_s)$ since the production is dominated by the strange quark fragmentation and the initial state Ξ^- contains twice as many s-quarks as Σ^-.

b) $\sigma(\Xi^- \to \overline{\Lambda}) = \sigma(\ \Sigma^- \to \overline{\Lambda})$ and $\sigma(\Xi^- \to \overline{\Xi}^+) = \sigma(\ \Sigma^- \to \overline{\Xi}^+)$ since the final state antiquarks are all new, thus the quark content of the initial state is unimportant.

The Σ^- interaction sample contains a K^- contamination of $(2.0 \pm 0.5)\%$. The V^0 production cross sections by K^- have been measured at beam momenta of up to 200 GeV/c [18] and these values were used for the correction. There exist no cross section measurements in K^- beams for $\overline{\Xi}^+$ or Ω^- production, therefore we assumed that the corresponding corrections were the same as for $\overline{\Lambda}$ or Ξ^-, i.e. 2% for $\overline{\Xi}^+$ and 0.4% for Ω^-,where the latter number was taken from [24].

Ξ^- decays upstream of the target are a source of Λ contamination in the neutron interaction sample. Since Σ^- and Ξ^- of equal momenta have practically equal decay lengths, the ratio of Λ to neutron flux is the same as the ratio of Ξ^- to Σ^- flux, i.e. 1.3% (see above). The production cross section of Λ by Λ is not known, therefore we used the production cross section of the very similar process $\Sigma^- \to \Sigma^-$ [34]. The resulting correction to the Λ production cross section is 4%. For $\overline{\Lambda}$, K^0_S and $\overline{\Xi}^+$ this contribution is negligibly small.

Table 2. The systematic contribution of different beam componets to the production cross section of strange particles integrated over the range $x_f > 0$ in %

	Σ^- beam components		neutron beam components
	K^-	Ξ^-	Λ
Λ	3.7	2.5	4.
$\overline{\Lambda}$	2.	1.3	-
K^0_S	5.	2.5	-
$\overline{\Xi}^+$	2.	1.3	-
Ω^-	0.4	-	-

The corrections from different beam components have been applied to the production cross sections. These correction values are shown in Table 2.

To estimate the uncertainties of the integrated cross sections we repeated the analysis with different sets of cuts applied for the V^0, $\overline{\Xi}^+$ and Ω^- identification. We changed the fiducial volume for the V^0 decays, the requirement on the distance between tracks at the V^0 decay vertex and the allowed range for the reconstructed effective V^0 mass. For the modified cuts the cross section result changed between -3.5 and 5.5%. We varied the equivalent criteria for the $\overline{\Xi}^+$ and Ω^- reconstruction. Here the resultant changes in the cross section were again of the order of $\pm 5\%$.

Finally the requirements on the quality of the interaction point were varied. With different cuts on the distance between the beam track and the reconstructed main vertex and on the distance between the tracks used in the main vertex fit variations of final the cross section result of $\pm 4\%$ were observed. Since we can not exclude that some of these uncertainties are correlated we add them linearly and obtained $\sigma = 15\%$. The detector simulation included the detector elements used for the trigger. To study the systematics of the trigger simulation we compared the response of this detector elements for events with an identified V^0 in beam trigger events with simulated events of the same type. The simulated trigger reproduces the trigger response found in real events within $\pm 7\%$. A small dependency on the general event multiplicity was found. We therefore assigned a total systematic error of $\sigma = 10\%$ to the uncertainties in the simulation of the trigger efficency. Since the beam trigger data sample was too small for the $\overline{\Xi}^+$ and Ω^- identification, we estimated the trigger efficency for $\overline{\Xi}^+$ and Ω^- as $\sigma = 10\%$ with the simulation only.

To check the time dependence of the detector and trigger efficiencies for our data taking we performed the analysis on subsamples. The observed variations correspond to an uncertainty of $\sigma \approx 5\%$ on the total result.

Table 3. Differential cross section of Λ production in copper and carbon as a function of x_F in mb

Beam	Neutrons		π^-		Σ^-	
x_F	Copper	Carbon	Copper	Carbon	Copper	Carbon
0.0–0.1	158. ± 2.	46. ± 1.	89. ± 1.	25.4± 0.3	164.± 2.	50. ± 1.
0.1–0.2	136. ± 1.	40.6± 0.4	62. ± 1.	19.4± 0.2	200.± 2.	65. ± 1.
0.2–0.3	94. ± 1.	30.0± 0.3	35.9± 0.4	11.6± 0.1	193.± 2.	69. ± 1.
0.3–0.4	65. ± 1.	22.8± 0.2	22.5± 0.2	7.7± 0.1	166.± 2.	65. ± 1.
0.4–0.5	43. ± 1.	16.7± 0.2	14.0± 0.2	6.0± 0.1	135.± 1.	56. ± 1.
0.5–0.6	27.5± 0.3	12.3± 0.1	10.7± 0.1	4.3± 0.1	105.± 1.	45. ± 1.
0.6–0.7	18.1± 0.3	7.9± 0.1	7.7± 0.1	3.5± 0.1	81.± 1.	36.1± 0.4
0.7–0.8	14.1± 0.3	4.9± 0.1	6.3± 0.2	2.1± 0.1	56.± 1.	26.7± 0.3

Table 4. Differential cross section of Λ production in copper and carbon as a function of p_t^2 in mb

Beam	Neutrons		π^-		Σ^-	
p_t^2	Copper	Carbon	Copper	Carbon	Copper	Carbon
0.0–0.2	104. ± 1.	35.8 ± 0.4	45.6 ± 0.5	15.6 ± 0.2	214. ± 2.	84. ± 1.
0.2–0.4	63. ± 1.	20.3 ± 0.2	26.4 ± 0.3	8.9 ± 0.1	125. ± 1.	47.8 ± 0.5
0.4–0.6	38.8± 0.4	12.6 ± 0.1	16.7 ± 0.2	5.4 ± 0.1	75. ± 1.	28.1 ± 0.3
0.6–0.8	24.9± 0.3	7.9 ± 0.1	10.5 ± 0.1	3.3 ± 0.03	46.6 ± 0.5	17.2 ± 0.2
0.8–1.0	16.4± 0.2	5.0 ± 0.1	6.7 ± 0.1	2.05± 0.02	29.8 ± 0.3	10.5 ± 0.1
1.0–1.2	10.5± 0.1	3.29± 0.04	4.8 ± 0.1	1.40± 0.02	19.4 ± 0.2	6.7 ± 0.1
1.2–1.4	6.8± 0.1	2.05± 0.03	3.6 ± 0.1	0.92± 0.01	13.4 ± 0.1	4.46± 0.04
1.4–1.6	5.7± 0.1	1.44± 0.02	2.50± 0.04	0.64± 0.01	9.4 ± 0.1	3.05± 0.03
1.6–1.8	4.1± 0.1	1.01± 0.02	1.82± 0.03	0.52± 0.01	6.5 ± 0.1	2.14± 0.02
1.8–2.0	3.0± 0.1	0.73± 0.02	1.37± 0.03	0.37± 0.01	5.10± 0.05	1.53± 0.02
2.0–2.2	2.0± 0.1	0.66± 0.02	1.10± 0.03	0.32± 0.01	3.73± 0.04	1.22± 0.01

Table 5. Differential cross section of $\overline{\Lambda}$ production in copper and carbon as a function of x_F in mb

Beam	Neutrons		π^-		Σ^-	
x_F	Copper	Carbon	Copper	Carbon	Copper	Carbon
0.0–0.1	46.8± 0.5	14.8 ± 0.2	55.6± 0.6	16.7 ± 0.2	42.1 ± 0.4	12.9 ± 0.1
0.1–0.2	21.3± 0.2	6.5 ± 0.1	35.0± 0.4	10.4 ± 0.1	19.3 ± 0.2	6.3 ± 0.1
0.2–0.3	7.1± 0.1	1.77± 0.04	17.3± 0.2	4.9 ± 0.1	6.2 ± 0.1	2.02 ± 0.02
0.3–0.4	1.4± 0.1	0.77± 0.04	6.6± 0.1	2.34± 0.04	1.49± 0.02	0.54 ± 0.01
0.4–0.5	–	–	2.8± 0.1	1.03± 0.03	0.57± 0.02	0.19 ± 0.01
0.5–0.6	–	–	1.3± 0.1	0.42± 0.03	0.26± 0.02	0.10 ± 0.01
0.6–0.7	–	–	0.3± 0.1	0.08± 0.04	0.06± 0.01	–
0.7–0.8	–	–	–	–	0.03± 0.02	0.011± 0.006

Adding all systematic errors quadratically we derive a total systematic uncertainty of $\sigma = 20\%$.

The corrected differential production cross sections are shown in Fig. 4–8 and listed in Tables 3–14 for copper and carbon targets. Only statistical errors are quoted here.

The cross sections were parameterized by a function of the form:

$$\frac{d^2\sigma}{dp_t^2 dx_F} = C(1-x_F)^n \cdot exp(-Bp_t^2), \qquad (2)$$

which is based on quark counting rules and phase space arguments [35]. The shape parameters n and B were assumed to be independent of p_t^2 and x_F. The solid lines on the graphs are shown in the region where this parametrisation gives a good description of the data and the extrapolation beyond the fit range is shown by the dashed lines. No significant difference is observed between the values obtained from the copper and the carbon target. The values of n and B obtained from the fits are listed in Table 15 for each target. In Fig. 9 we show the cross sections for V^0 production by Σ^- as a function of p_t^2 up to 4 $(\mathrm{GeV}/c)^2$. The distributions were parameterized by three different functions:

a) $\mathrm{d}\sigma/\mathrm{d}p_T^2 \propto exp(-Bp_T^2)$: Gaussian.
b) $\mathrm{d}\sigma/\mathrm{d}p_T^2 \propto exp(-bp_T)$: non-Gaussian tails at high p_T (dashed line b).
c) $\mathrm{d}\sigma/\mathrm{d}p_T^2 \propto m_T^{3/2} exp(-m_T/kT)$: "thermal distribution" (dot-dashed line c).

Table 6. Differential cross section of $\overline{\Lambda}$ production in copper and carbon as a function of p_t^2 in mb

Beam	Neutrons		π^-		Σ^-	
p_t^2	Copper	Carbon	Copper	Carbon	Copper	Carbon
0.0–0.2	17.3 ± 0.2	5.8 ± 0.1	23.7 ± 0.2	7.4 ± 0.1	14.2 ± 0.1	4.70 ± 0.05
0.2–0.4	8.7 ± 0.1	2.85± 0.04	13.9 ± 0.1	4.21± 0.04	7.9 ± 0.1	2.45 ± 0.03
0.4–0.6	5.3 ± 0.1	1.27± 0.02	8.2 ± 0.1	2.39± 0.03	4.5 ± 0.05	1.44 ± 0.02
0.6–0.8	2.54± 0.05	0.87± 0.02	4.82± 0.06	1.36± 0.02	2.91 ± 0.03	0.91 ± 0.01
0.8–1.0	1.39± 0.04	0.46± 0.01	3.20± 0.04	0.98± 0.01	1.85 ± 0.02	0.57 ± 0.01
1.0–1.2	1.06± 0.03	0.29± 0.01	2.05± 0.03	0.60± 0.01	1.24 ± 0.01	0.335± 0.004
1.2–1.4	0.80± 0.03	0.19± 0.01	1.67± 0.03	0.40± 0.01	0.83 ± 0.01	0.245± 0.003
1.4–1.6	0.42± 0.03	0.11± 0.01	1.03± 0.02	0.30± 0.01	0.56 ± 0.01	0.171± 0.002
1.6–1.8	0.36± 0.03	0.07± 0.01	0.80± 0.02	0.22± 0.01	0.43 ± 0.01	0.121± 0.002
1.8–2.0	0.21± 0.02	0.05± 0.01	0.57± 0.02	0.13± 0.01	0.275± 0.004	0.092± 0.001
2.0–2.2	0.13± 0.02	0.03± 0.01	0.34± 0.02	0.11± 0.01	0.246± 0.004	0.063± 0.001

Table 7. Differential cross section of K^0 production in copper and carbon as a function of x_F in mb

Beam	Neutrons		π^-		Σ^-	
x_F	Copper	Carbon	Copper	Carbon	Copper	Carbon
0.0–0.1	279. ± 3.	86. ± 1.	244. ± 2.	79. ± 1.	285. ± 3.	94. ± 1.
0.1–0.2	146. ± 2.	48. ± 1.	156. ± 2.	51. ± 1.	205. ± 2.	68. ± 1.
0.2–0.3	60. ± 1.	18.8± 0.2	75. ± 1.	25.0± 0.3	104. ± 1.	36.1± 0.4
0.3–0.4	23.8± 0.3	8.6± 0.1	35.3± 0.4	11.8± 0.1	46.2± 0.5	16.3± 0.2
0.4–0.5	9.1± 0.2	3.3± 0.1	14.5± 0.2	5.0± 0.1	14.5± 0.1	5.7± 0.1
0.5–0.6	4.1± 0.2	1.9± 0.1	6.7± 0.1	2.1± 0.1	5.2± 0.1	1.8± 0.1
0.6–0.7	–	–	9.3± 0.2	1.6± 0.1	5.3± 0.1	1.0± 0.1

Table 8. Differential cross section of K^0 production in copper and carbon as a function of p_t^2 in mb

Beam	Neutrons		π^-		Σ^-	
p_t^2	Copper	Carbon	Copper	Carbon	Copper	Carbon
0.0–0.2	118. ± 1.	38.6 ± 0.4	120. ± 1.	40.4 ± 0.4	148. ± 1.	51.7 ± 0.5
0.2–0.4	55.9 ± 0.6	18.2 ± 0.2	58.9 ± 0.6	19.5 ± 0.2	73.6 ± 0.7	24.8 ± 0.3
0.4–0.6	30.6 ± 0.3	9.5 ± 0.1	32.2 ± 0.3	10.2 ± 0.1	40.5 ± 0.4	13.3 ± 0.1
0.6–0.8	19.4 ± 0.2	5.56± 0.06	20.4 ± 0.2	5.73± 0.06	23.9 ± 0.2	7.8 ± 0.1
0.8–1.0	10.9 ± 0.1	3.52± 0.04	12.5 ± 0.1	3.61± 0.04	15.6 ± 0.2	4.69± 0.05
1.0–1.2	8.3 ± 0.1	2.47± 0.03	7.6 ± 0.1	2.40± 0.03	10.3 ± 0.1	3.16± 0.03
1.2–1.4	5.1 ± 0.1	1.48± 0.03	6.1 ± 0.1	1.64± 0.02	7.2 ± 0.1	2.15± 0.02
1.4–1.6	3.4 ± 0.1	1.28± 0.02	4.20± 0.05	1.33± 0.02	5.31± 0.05	1.48± 0.02
1.6–1.8	2.92± 0.06	0.79± 0.02	2.83± 0.04	0.96± 0.01	3.79± 0.04	1.07± 0.01
1.8–2.0	2.36± 0.06	0.52± 0.02	2.37± 0.04	0.57± 0.01	2.80± 0.03	0.83± 0.02
2.0–2.2	1.36± 0.05	0.36± 0.02	2.03± 0.04	0.51± 0.01	2.16± 0.02	0.60± 0.01

Table 9. Differential cross section of Λ, $\overline{\Lambda}$ and K^0 production by Σ^- in copper and carbon as a function of p_t^2 in mb

	Λ		$\overline{\Lambda}$		K^0	
x_F	Copper	Carbon	Copper	Carbon	Copper	Carbon
2.2–2.4	2.95 ± 0.03	0.858 ± 0.009	0.167 ± 0.003	0.048 ± 0.001	1.74 ± 0.02	0.459 ± 0.005
2.4–2.6	2.21 ± 0.02	0.638 ± 0.007	0.153 ± 0.003	0.037 ± 0.001	1.40 ± 0.02	0.359 ± 0.004
2.6–2.8	1.91 ± 0.02	0.505 ± 0.006	0.116 ± 0.003	0.024 ± 0.001	1.08 ± 0.01	0.321 ± 0.004
2.8–3.0	1.49 ± 0.02	0.430 ± 0.005	0.104 ± 0.003	0.026 ± 0.001	1.02 ± 0.01	0.245 ± 0.003
3.0–3.2	1.27 ± 0.02	0.338 ± 0.004	0.088 ± 0.003	0.021 ± 0.001	0.73 ± 0.01	0.209 ± 0.003
3.2–3.4	1.05 ± 0.01	0.281 ± 0.004	0.080 ± 0.003	0.013 ± 0.001	0.67 ± 0.01	0.159 ± 0.003
3.4–3.6	0.88 ± 0.01	0.246 ± 0.004	0.029 ± 0.002	0.013 ± 0.001	0.58 ± 0.01	0.130 ± 0.002
3.6–3.8	0.68 ± 0.01	0.176 ± 0.003	0.022 ± 0.002	0.007 ± 0.001	0.43 ± 0.01	0.103 ± 0.002
3.8–4.0	0.56 ± 0.01	0.149 ± 0.003	0.032 ± 0.003	0.007 ± 0.001	0.36 ± 0.01	0.086 ± 0.002

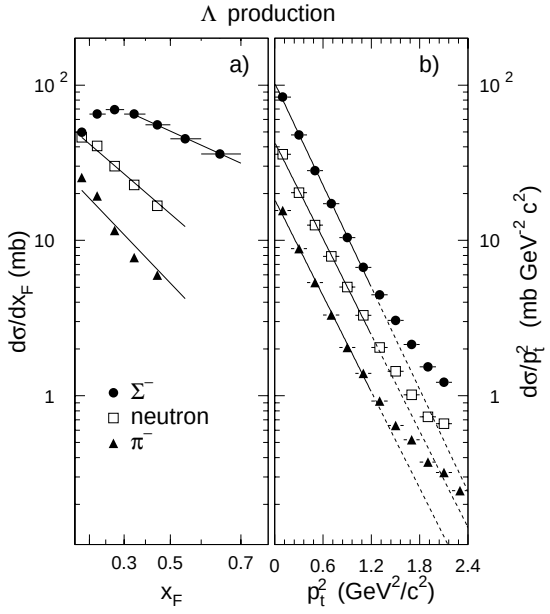

Fig. 4a,b. Differential cross sections of inclusive Λ production by Σ^-, π^- and neutrons in carbon. The straight line shows the result of the fit. The dashed line shows the extrapolaion of the fit beyond the fit region

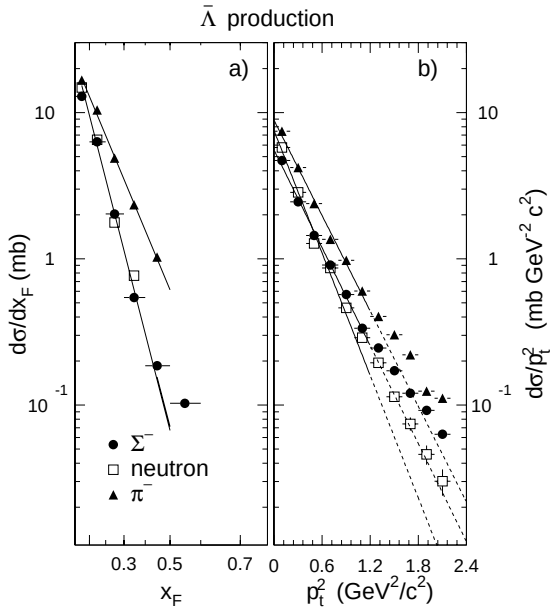

Fig. 6a,b. Differential cross sections of inclusive $\overline{\Lambda}$ production by Σ^-, π^- and neutrons in carbon. The straight line shows the result of the fit. The dashed line shows the extrapolaion of the fit beyond the fit region

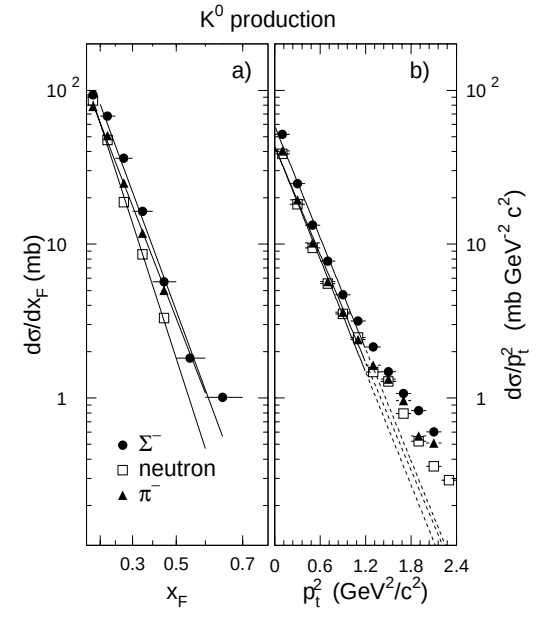

Fig. 5a,b. Differential cross sections of inclusive K^0_S production by Σ^-, π^- and neutrons in carbon. The straight line shows the result of the fit. The dashed line shows the extrapolaion of the fit beyond the fit region

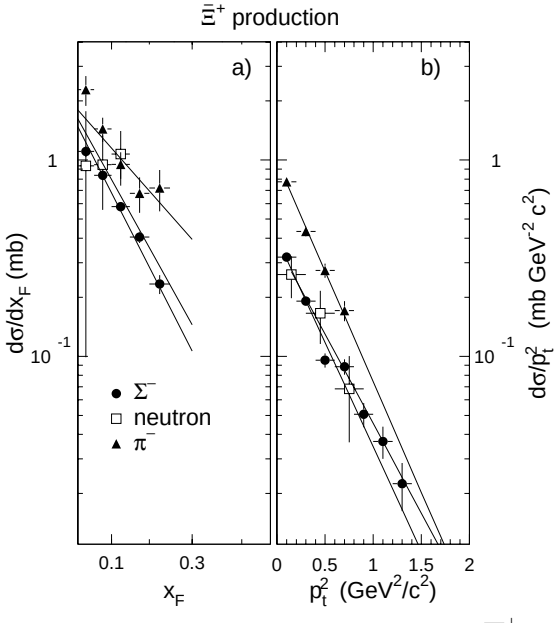

Fig. 7a,b. Differential cross sections of inclusive $\overline{\Xi}^+$ production by Σ^-, π^- and neutrons in carbon. The straight line shows the result of the fit

Figure 9 shows that neither a pure Gaussian nor a single thermal distribution can describe the observed p_t^2 spectra. The exponential ansatz b) gives a reasonable fit to the spectrum at high p_t^2, only at very low p_t^2 is the experimental slope less steep than the fit.

In Fig. 10 we present B values from a Gaussian fit ("a" in Fig. 9) to all p_t^2 distributions of strange particles observed in our experiment as a function of the particle mass [24,34,36–38]. The B values decrease with increasing mass and can be fit by the simple formula: $B \propto C_1 - C_2 \cdot M^{\delta}$ where $\delta = 4.1 \pm 0.1$. It is very interesting to compare this behavior with predictions based on the thermal model (for example [39]). We tried different parameterizations for the p_t^2 distribution, such as $w \propto exp(-\sqrt{p_t^2 + M^2}/T)$, where T denotes a temperature or a more sophisticated expression involving the chemical potential. All parameteriza-

Table 10. Differential cross section of Ω^- production by Σ^- in copper and carbon as a function of x_F in mb

x_F	copper	carbon
0.00–0.15	1.29 ± 0.1	0.37 ± 0.03
0.15–0.30	1.38 ± 0.05	0.33 ± 0.02
0.30–0.45	1.14 ± 0.05	0.31 ± 0.02
0.45–0.60	0.42 ± 0.05	0.13 ± 0.01

Table 11. Differential cross section of Ω^- production by Σ^- in copper and carbon as a function of p_t^2 in mb/(GeV/c)^2

p_t^2	copper	carbon
0.00–0.40	0.66 ± 0.05	0.17 ± 0.02
0.40–0.80	0.48 ± 0.04	0.12 ± 0.02
0.80–1.20	0.23 ± 0.03	0.06 ± 0.01
1.20–1.60	0.08 ± 0.03	0.04 ± 0.01
1.60–2.00	0.04 ± 0.03	0.03 ± 0.01

Table 12. Differential cross section of $\overline{\Xi}^+$ production as a function of x_F in mb

Beam	Neutrons		π^-		Σ^-	
x_F	Copper	Carbon	Copper	Carbon	Copper	Carbon
0.00–0.05	6. ± 3.	0.9 ± 0.8	4.8 ± 0.9	2.3 ± 0.4	4.4 ± 0.3	1.11 ± 0.04
0.05–0.10	6. ± 2.	0.9 ± 0.4	3.5 ± 0.5	1.4 ± 0.2	2.9 ± 0.1	0.84 ± 0.04
0.10–0.15	3.7± 0.9	1.1 ± 0.3	3.7 ± 0.5	0.9 ± 0.2	1.8 ± 0.1	0.58 ± 0.03
0.15–0.20	–	–	2.6 ± 0.5	0.7 ± 0.1	1.3 ± 0.1	0.40 ± 0.03
0.20–0.25	–	–	2.1 ± 0.5	0.7 ± 0.2	0.97± 0.08	0.23 ± 0.03
0.25–0.30	–	–	1.5 ± 0.5	0.5 ± 0.2	0.26± 0.07	0.06 ± 0.02

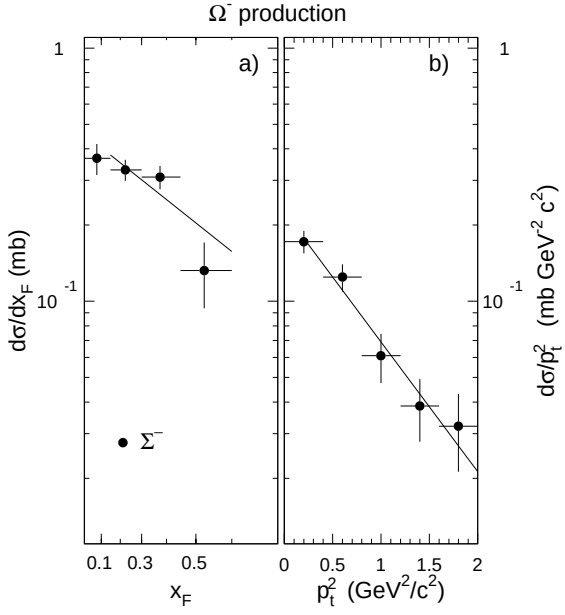

Fig. 8a,b. Differential cross sections of inclusive Ω^- production by Σ^- in carbon. The straight line shows the result of the fit

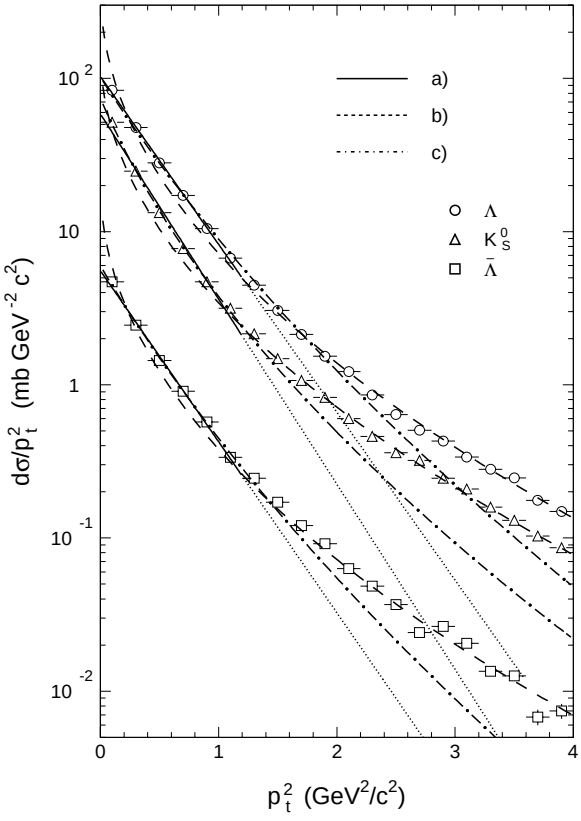

Fig. 9. The differential production cross section of V^0 as a function of p_t^2 produced in Σ^- interactions. The straight line shows the result of the Gaussian fit. The doted line shows the extrapolaion of the Gaussian fit beyond the fit region. See text for the meaning of other lines

tions yield results very different from the observations – the curvatures of the functions have a different sign.

Figure 11 shows the nuclear mass dependence of V^0 and cascade hyperon production as a function of x_F (left) and p_t^2 (right). The left-hand scales give the cross section ratio:

$$R = \frac{\sigma_{Cu}}{\sigma_C} \cdot \frac{A_C}{A_{Cu}} \tag{3}$$

The right-hand scales shows the corresponding values of α in the conventional parameterization for the A dependence:

$$\sigma = \sigma_0 \cdot A^\alpha \tag{4}$$

The dashed lines correspond to α=2/3 and α=1, respectively.

The values for V^0 and cascade hyperon production are very similar to each other and to those observed in other

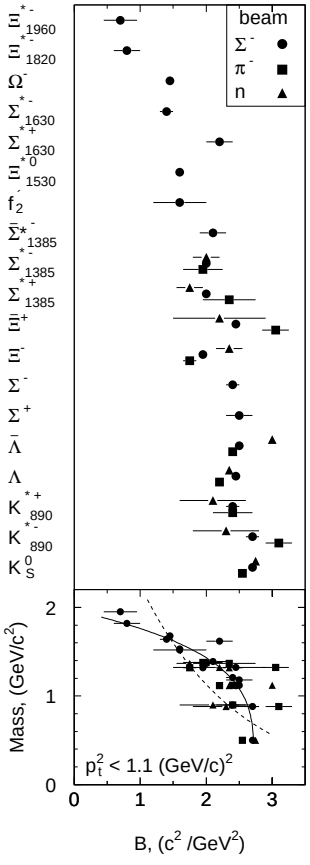

Fig. 10. The B parameter values (see (2)) for different particles (*top*); the B parameter as a function of the mass (*bottom*). The solid line is a fit of experimental data, the dushed line is the thermal model prediction

Table 13. Differential cross section of $\overline{\Xi}^+$ production by π^- , Σ^- as a function of p_t^2 in mb/(GeV/c)^2

Beam	π^-		Σ^-	
x_F	Copper	Carbon	Copper	Carbon
0.0–0.2	2.43 ± 0.08	0.78 ± 0.03	1.13 ± 0.04	0.32 ± 0.01
0.2–0.4	1.19 ± 0.07	0.43 ± 0.03	0.71 ± 0.03	0.19 ± 0.01
0.4–0.6	0.57 ± 0.06	0.27 ± 0.02	0.40 ± 0.03	0.10 ± 0.01
0.6–0.8	0.40 ± 0.06	0.17 ± 0.02	0.27 ± 0.03	0.09 ± 0.01
0.8–1.0	–	–	0.16 ± 0.02	0.05 ± 0.01
1.0–1.2	–	–	0.15 ± 0.02	0.04 ± 0.01
1.2–1.4	–	–	0.09 ± 0.02	0.02 ± 0.01

Table 14. Differential cross section of $\overline{\Xi}^+$ production by neutron as a function of p_t^2 in mb/(GeV/c)^2

p_t^2	copper	carbon
0.00–0.30	1.4 ± 0.3	0.26 ± 0.06
0.30–0.60	0.9 ± 0.2	0.17 ± 0.05
0.60–0.90	0.3 ± 0.2	0.07 ± 0.03

hadroproduction processes which can be summarized as $\alpha(x_F) = 0.8 - 0.75x_F + 0.45x_F^2$ [40] (solid line in the left part of Fig. 11). For K_S^0 produced by Σ^- a strong deviation in the α value is seen at x_F= 0.65. The deviation of this point is probably due to a fluctuation at the edge of the spectrometer acceptance.There is no visible dependence of α on p_t^2.

The production cross sections per nucleus integrated over all p_t^2 and $x_F > 0$ are listed in Table 1 for the copper and carbon targets separately. These production cross section were fit by $\sigma_0 \cdot A^\alpha$ function and the fit values for the cross sections per nucleon and α are also shown in the Table 1. The errors listed in the table are statistical errors only.

6 Discussion

We first discuss the features of the p_t^2 spectra. The first observation of V^0 p_t^2 spectra over such a wide range of p_t^2 1–4 (GeV/c)^2 shows that the Gaussian or "thermal" approximations are only valid in the region below 1.0-1.2 (GeV/c)^2. Thus the approximations made in the 'thermal" model as proposed in [39] have to be considered very carefully.

In total, experiment WA89 has provided production cross sections for 19 strange particles. It is interesting to study the slope parameters of the p_t^2 spectra as a function of the mass of the particle produced. For this dependence, the thermal model predicts a curvature opposite in sign to the experimental behavior (Fig. 10). The difference in curvature cannot be changed by varying the parameters of the model. Thus the swap of the curvature sign can be considered as the reliable signature of the thermalization of the system.

We now turn to the x_F spectra. The x_F-dependence of the invariant production cross sections clearly shows the leading particle effect (Fig. 12) which depends on the overlap of the quark contents in the beam particle and the particle produced: more overlap results in harder x_F distributions.

We have compared the experimental results with theoretical calculations based on PYTHIA 5.7 and JETSET 7.4 [41] and the Quark-Gluon String Model (QGSM, see [42], [43] and references therein).

PYTHIA was used with its default set of parameters, and no attempt was made to adjust them to obtain a better fit of the experimental data. In the PYTHIA calculations, elastic and diffraction processes were included (PYTHIA option `MSEL=2`) and the Lund string fragmentation algorithm was used. The latter is more similar to the QGSM model than "independent" or "cluster" fragmentation.

In the QGSM, a baryon may be produced either directly from the projectile diquark, or indirectly in a remote part of the color string (this includes quark, antiquark and antidiquark fragmentation cases). Similarly, the model distinguishes between the production of K mesons from strange and non-strange constituents. Although the

Table 15. The fit parameter values of the differential cross section approximation in form of $d^2\sigma/dp_t^2dx_F = C(1-x_F)^n exp(-Bp_t^2)$ with their fit errors (see text)

	Beam	Σ^-		π^-		Neutrons	
	target	n	B	n	B	n	B
Λ	Cu	1.13 ± 0.01	2.40 ± 0.01	2.71 ± 0.02	2.17 ± 0.01	2.23 ± 0.02	2.27 ± 0.01
	C	0.93 ± 0.01	2.52 ± 0.01	2.12 ± 0.02	2.33 ± 0.01	1.80 ± 0.02	2.38 ± 0.01
$\overline{\Lambda}$	Cu	8.57 ± 0.04	2.44 ± 0.01	5.53 ± 0.04	2.35 ± 0.01	8.18 ± 0.08	3.03 ± 0.03
	C	8.20 ± 0.04	2.57 ± 0.01	5.23 ± 0.04	2.47 ± 0.01	8.46 ± 0.09	3.22 ± 0.03
K^0	Cu	5.38 ± 0.02	2.64 ± 0.01	4.94 ± 0.02	2.52 ± 0.01	6.39 ± 0.03	2.72 ± 0.02
	C	5.26 ± 0.02	2.78 ± 0.01	4.92 ± 0.02	2.67 ± 0.01	6.02 ± 0.03	2.82 ± 0.02
$\overline{\Xi}^+$	Cu	7.8 ± 0.1	2.45 ± 0.05	$4. \pm 1.$	3.2 ± 0.3	$6. \pm 3.$	2.3 ± 0.7
	C	7.4 ± 0.1	2.45 ± 0.05	$4. \pm 1.$	2.6 ± 0.3	$5. \pm 4.$	2.1 ± 0.8
Ω^-	Cu	1.65 ± 0.07	1.55 ± 0.06	–	–	–	–
	C	1.20 ± 0.08	1.26 ± 0.05	–	–	–	–

absolute normalization of these contributions is arbitrary, their x_F behavior is strictly defined in the model. We have used the normalization freedom to tune the parameters to the process $nC \to \Lambda X$. Once fixed, the parameters remain unchanged whatever other projectile particles come into play.

Both models, PYTHIA and QGSM, reproduce the hardness hierarchy in the x_F distributions of V^0 production (Fig. 13). Production by π^- and Σ^- yields similar K^0_S spectra, while neutrons yield a softer spectrum. Also, neutrons and Σ^- yield similar $\overline{\Lambda}$ spectra, while pions yield a harder spectrum. Finally, the Λ hardness degrades from Σ^- to n and further to π^- beam particles.

The most significant discrepancies between the models and the data are seen in the Λ spectra. PYTHIA seems to show a too strong leading particle effect for Σ^- and n beams, while the QGSM seems to show a too small difference between the Σ^- and n cases. The similarity between the Σ^- and n-induced spectra in the QGSM comes from the fact that baryon-to-baryon fragmentation is greatly influenced by the transmission of the string junction. At low and moderate x_F, this factor appears to be even more important than the baryon flavor content — a feature that we have already pointed out in a previous publication (regarding Ξ^- production by neutrons) [24].

Concerning the $\overline{\Lambda}$ spectra, the suppression of antibaryon production by Σ^- or n relative to the baryon production is evident and well reproduced by both models.

The data show a difference between the x_F spectra of Λ and $\overline{\Lambda}$ produced by pions. This is completely unexpected because the baryon and antibaryon valence quark overlap with the π^- is symmetric. Therefore their production spectra should be identical at least in the positive x_F region where the target role is negligible.

For K^0_S production, the agreement between data and model calculations is also better than for Λ production.

A qualitative explanation of the K^0_S x_F -spectra within the QGSM may be given as follows. The fragmentation of a baryon into a meson is disfavored because of the necessity to remove the valence diquark with its color string junction from the projectile. This must equally soften the kaon spectra in the n and Σ^- beams, but the suppression does not apply to the π^- beam. On the other hand, the presence of a strange quark in the Σ^- beam particle opens the way for direct fragmentation (enhanced by a numerically large normalizing coefficient in QGSM). Thus, the strangeness overcomes the disfavor of Σ^- fragmentation. The fragmentation of neutrons is left with no compensation.

The comparison between models and data for $\overline{\Xi}^+$ and Ω^- production is straightforward. All constants in the QGSM model were already fixed in our previous studies of Ξ^- production [24]. Both models fail on the magnitude of the production cross sections. The x_F distributions of $\overline{\Xi}^+$ production are somewhat better reproduced by PYTHIA than by the QGSM, the inverse holds for Ω^- production (Fig. 14).

The transverse momentum distributions show weak dependence on the beam type. The p_T^2 spectra generated by PYTHIA are systematically narrower than the data and the spectra generated by the QGSM, although the algorithm that could provide the p_T broadening was turned on (i.e. the initial and final state parton showering, PYTHIA options `MSTP(61)=1`, `MSTP(71)=1`). This may be related to the fact that much of the production cross section is due to quasielastic and diffractive contributions. In the QGSM, the p_T behavior does not depend on the intrinsic features of the theory and is regulated by two free parameters.

7 Conclusion

We have observed clear signals of Λ, $\overline{\Lambda}$, K^0_S, $\overline{\Xi}^+$ and Ω^- produced by $\Sigma^-$and $\pi^-$of 345 GeV/c momentum and by neutrons of 260 GeV/c mean momentum in copper and carbon in the same experimental conditions. This gives us a unique possibility to study their production spectra.

The differential production cross sections as a function of x_F show the expected qualitative effect of the quark content overlap in the beam and produced particles with the only exception of the Λ and $\overline{\Lambda}$ in π^- induced interactions.

The p_t^2 spectra are well parameterized by Gaussian function in the p_t^2 region below 1.1 (GeV/c)^2. The V^0 spectra flatten substantially above 1.2 (GeV/c)^2 showing

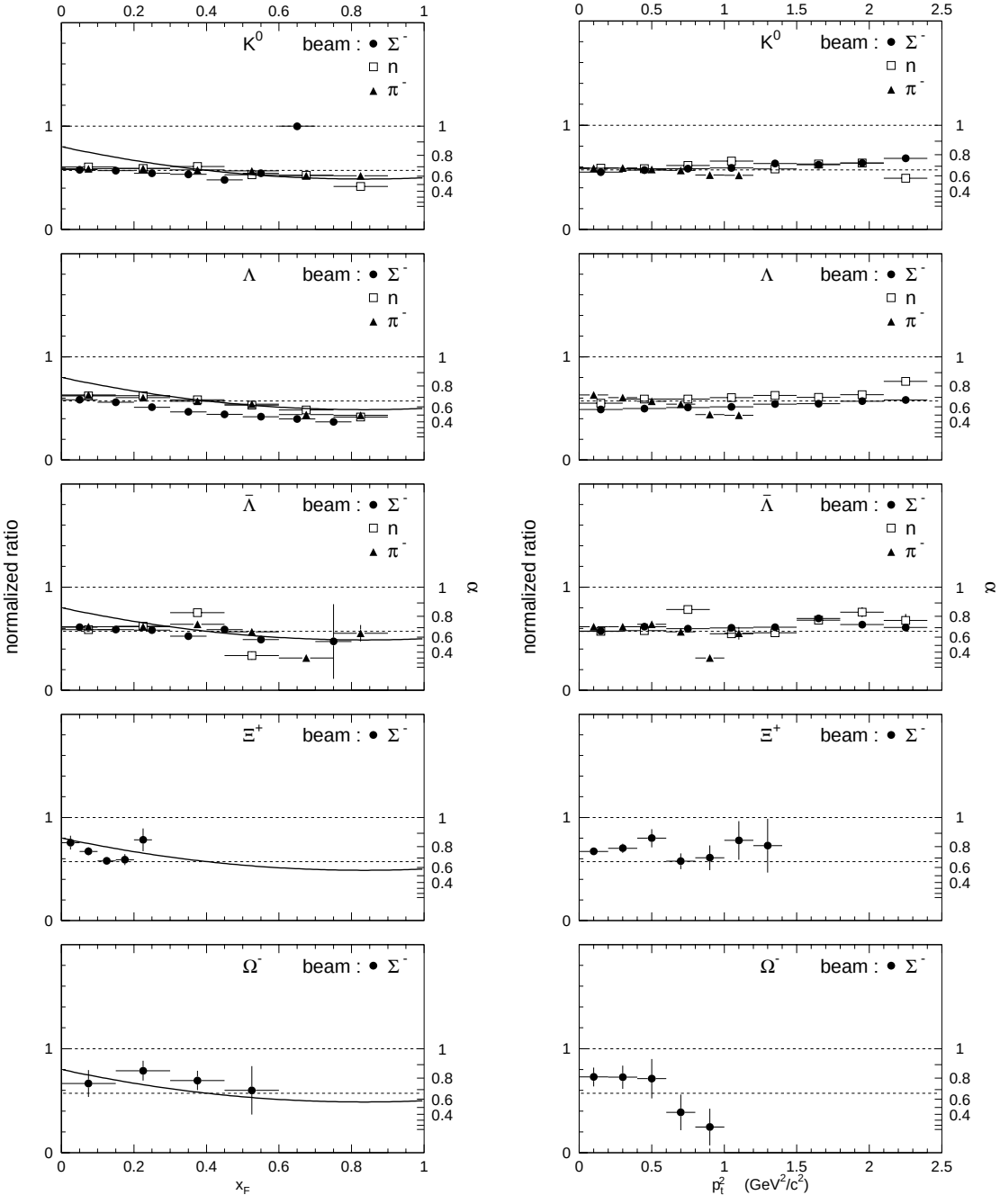

Fig. 11. Normalized ratio R (see (3)) of V^0's and cascade hyperon production by Σ^-, π^- and netrons in copper and carbon as a function of x_F (left) and p_t^2 (right). The right scale indicates the exponent α in the A^α dependence. The solid lines in the left part show a polynomial fit to a compilation of target attenuation factors given in [40]. The dashed horisontal lines indicate the limiting cases for α= 2/3 (strong attenuation) and α= 1 (no attenuation)

the same trend as other particles studied in the experiment [24,34,38]. The fit parameter B of the Gaussian function decreases with the increase of the particle mass. The comparison of our result with the thermal model calculation shows that thermalization did not happens in our experimental condition. We could expect that the shape of the experimental and theoretical curve will be similar at other experimental conditions, for example in heavy ion collision.

The A^α dependence of all production cross sections is consistent with hypotheses of $\alpha \approx 2/3$ for produced and beam particles.

To summarize, the abundant data on hyperon and K^0_S hadroproduction now available cannot yet be satisfactorily described by existing phenomenological models. A better understanding of these processes is desirable not only by itself, but also for extrapolations to other energy regions.

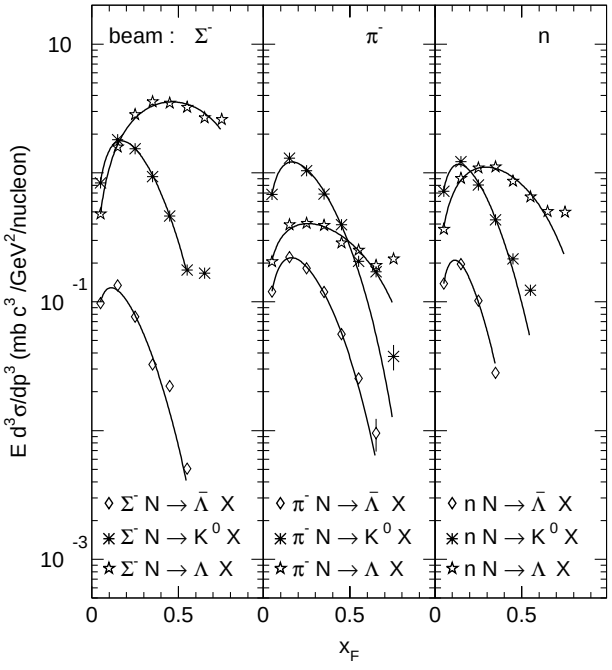

Fig. 12. The V^0 invariant production cross section in Σ^-, π^- and neutron beams. The lines have been drawn to guide the eye

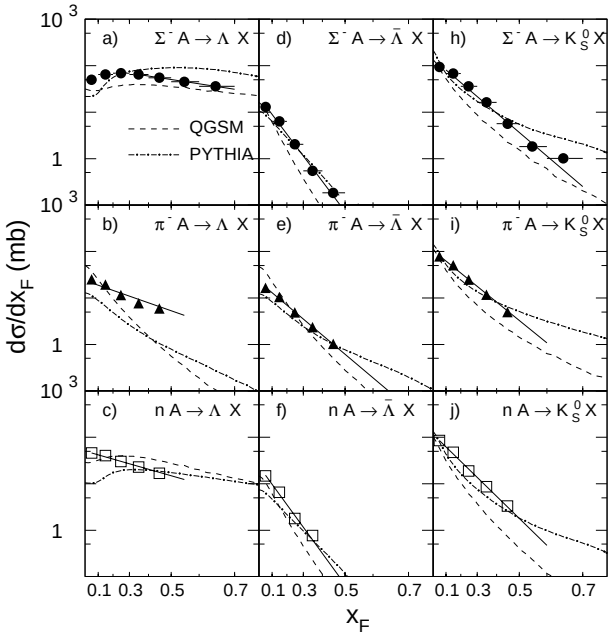

Fig. 13a–j. The comparison of the measured differential cross section with PYTHIA and QGSM prediction for V^0 hyperon production in Σ^-, π^- and neutron beams. The solid line shows the the result of the fit by $\propto (1 - x_F)^n$

Acknowledgements. It is a pleasure to thank J. Zimmer and G. Konorova for their support in setting up and running the experiment. We are also indebted to the staff of the CERN Omega spectrometer group for their help and support, to the CERN EBS group for their work on the hyperon beam line and to the CERN accelerator group for their continuous efforts to provide good and stable beam conditions. Yu. Alexandrov and S. Baranov are grateful for the support by the Deutsche Forschungsgemeinschaft and the Russian Foundation for Basic Research under contract numbers 436 RUS 113/465.

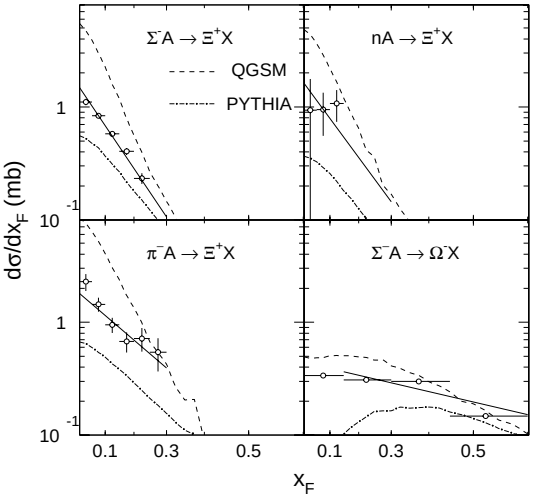

Fig. 14. The comparison of the measured differential cross section with PYTHIA and QGSM prediction for cascade hyperon production. The solid line shows the the result of the fit by $\propto (1 - x_F)^n$

References

1. S.Erhan et al., Phys. Lett. B **85**, 447 (1979)
2. P.Skubic et al., Phys. Rev. D **18**, 3115 (1978)
3. B.Y.Oh et al., Nucl. Phys. B **49**, 13 (1972)
4. M.Alston-Garnjost et al., Phys. Rev. Lett. **35**, 142 (1975)
5. K.Heller et al., Phys. Rev. D **16**, 2737 (1977)
6. A.Sheng et al., Phys. Rev. D **11**, 1733 (1975)
7. F.T.Dao et al., Phys. Rev. Lett. **30**, 1151 (1973)
8. J.W.Chapman et al., Phys. Lett. B **47**, 465 (1973)
9. H.Bøggild et al., Nucl. Phys. B **57**, 77 (1973)
10. V.Blobel et al., Nucl. Phys. B **69**, 454 (1974)
11. H.Kihimi et al., Phys. Lett. B **72**, 411 (1978)
12. K.Jaeger et al., Phys. Rev. D **11**, 1756 (1975)
13. K.Jaeger et al., Phys. Rev. D **11**, 2405 (1975)
14. S.Mikocki et al., Phys. Rev. D **34**, 42 (1986)
15. D.Bogert et al., Phys. Rev. D **16**, 2098 (1977)
16. D.Ljung et al., Phys. Rev. D **15**, 3163 (1977)
17. N.N.Biswas et al., Nucl. Phys. B **167**, 41 (1980)
18. R.T.Edwards et al., Phys.Rev. D **18**, 76 (1978)
19. A.Aleev et al., Yad.Fiz. **44**, 661 (1986); Sov.J.Nucl.Phys. **44**(3) (1986) 429
20. F.A.Dibianca et al., Nucl. Phys. B **98**, 137 (1975)
21. J.K.Hassall et al., Nucl. Phys. B **189**, 397 (1981)
22. M.Baubillier et al., Nucl. Phys. B **192**(1981) 1
23. D.Aston et al., Phys.Rew. D **32**, 2270 (1985)
24. Yu.A.Alexandrov et al., Z. Phys. C **76**, 35 (1997)
25. S.F.Biagi et al., Z. Phys. C **34**, 187 (1987)
26. T.R. Cardello et al., Phys. Rev. D **32**, 1 (1985)
27. S.Nagamiya, Nucl. Phys. **566**, 287c (1994)

28. J.W.Harris, Nucl. Phys. **566**, 277c (1994)
29. S.A.Bass et al., Nucl. Phys. A **661**, 205c (1999)
30. W.Brückner et al., Nucl. Instr. Meth. A **378** (1996) 451
31. Yu.A.Alexandrov et al., CERN-SL-97-60 EA Nucl. Instr. Meth. A **408**, 359 (1998)
32. W. Beusch, CERN/SPSC/77-70
33. The Particle Data Group, Eur. J. Phys, C **15** (2000) 1
34. Yu.A.Alexandrov et al., Eur. Phys. J. C **22**, (2001) 255
35. R. Blankenbecler and S.J. Brodsky, Phys. Rev. D **10**, 2973 (1974)
36. Yu.A.Alexandrov et al., Eur. J. Phys, C **5**, 621 (1998)
37. Yu.A.Alexandrov et al., Eur. Phys. J. C **11**, 271 (1999)
38. Yu.A.Alexandrov et al., Eur. Phys. J. C **22**, 47 (2001)
39. W.M.Geist et al., Z. Phys. C **71**, 45 (1996)
40. W.M. Geist, Nucl. Phys. A**525**, 149c (1991)
41. T. Sjöstrand, Computer Phys. Comm. **82**, 74 (1994)
42. A.B. Kaidalov and K.A. Ter-Martirosyan, Sov. J. Nucl. Phys. **39**, 1545 (1984) , A.I. Veselov, O.I. Piskunova and K.A. Ter-Martirosyan, Phys. Lett. B **158**, 175 (1985), A.B. Kaidalov and O.I. Piskunova, Z. Phys. C **30**, 145 (1986), A.B. Kaidalov, Sov. J. Nucl. Phys. **45**, 1450 (1987)
43. S.P. Baranov, Lebedev Institute of Physics report **42**, 1998